Directional anemometer based on an anisotropic flat-clad tapered fiber Michelson interferometer

Cheng-Ling Lee, Chung-Fen Lee, Chai-Ming Li, Tsai-Ching Chiang, and Ying-Li Hsiao

Citation: Applied Physics Letters **101**, 023502 (2012); doi: 10.1063/1.4734501
View online: http://dx.doi.org/10.1063/1.4734501
View Table of Contents: http://scitation.aip.org/content/aip/journal/apl/101/2?ver=pdfcov
Published by the AIP Publishing

Directional anemometer based on an anisotropic flat-clad tapered fiber Michelson interferometer

Cheng-Ling Lee,[a] Chung-Fen Lee, Chai-Ming Li, Tsai-Ching Chiang, and Ying-Li Hsiao
Department of Electro-Optical Engineering, National United University, Miaoli, 360 Taiwan

(Received 6 March 2012; accepted 23 June 2012; published online 10 July 2012)

This work demonstrates a sensitive directional anemometer that is based on a pendulum-type of anisotropic flat-clad tapered fiber Michelson interferometer (AFCTFMI). The AFCTFMI is fabricated by tapering an anisotropic flat-cladding fiber to establish structural anisotropy, and enables the sensing of the direction and magnitude of flowing air (wind). Wavelength shifts and fringes visibility of the measured interference fringes are correlated with the magnitude and furthermore the direction of the wind. Experimental results agree closely with the theoretical analysis. The directional anemometer can simultaneously and effectively indicate the direction, and sensitively measure the magnitude of wind. © *2012 American Institute of Physics*.
[http://dx.doi.org/10.1063/1.4734501]

An anemometer measures the speed of wind. This capability is very important in various applications. Methods of measurement that are based on fiber optics have attracted many interests because of the uniquely non-electrical operation of the fiber, compact optical wave-guiding and the fact that optical sensing can be performed over a long distance.[1–9] Lien and Vollmer reported a fiber-tipped cantilever sensing configuration for measuring the speed of flowing fluid. Optical light inputs an etched thinned fiber cantilever to reduce optical coupling of a receiving multi-mode fiber when the fluidic drag force acts on the fiber-tip to make a displacement of the emitting light from the fiber.[1] The well known fiber-based sensor for sensing fluid/wind is based on optical fiber Bragg gratings (FBGs).[2–5] Force that is exerted by a fluid bends or distorts FBGs under the strain. The measurement mechanism is sensitive, but requires temperature compensation, because FBGs are highly sensitive to ambient temperature.[2,3] Another type of optical FBG anemometer that measures wind by cooling thermal FBGs has been demonstrated for sensing air and electrical wind.[4,5] The above sensors are quite practical but fabrications of the devices are complicated: expensive lasers or integrated processes are required. Therefore, for simplicity, special fibers with specific characteristics have also been utilized to measure flow rates.[6,7] Another simple configuration of two aligned fiber endfaces as an air-gap fiber Fabry-Perot interferometer for the highly sensitive sensing of airflow has recently been proposed. Although this simple sensor is extremely sensitive, an alignment process is still required and the measurement range is limited.[8] Frazão *et al*. presented a tapered fiber with a length of 10 cm, which was inserted into a pressured air tube to sense flowing fluid. The horizontal fiber element is originally maximally bent under the weight of the fiber, and rises as the pressure of the air that is input to the tube increases, reducing the bending of the fiber. Since the fiber arm of the above sensor is parallel to the input flowing air, the sensor may suffer from a limited dynamic range or turbulence inside the tube when placed in fast flowing air.[9] The above fiber-optical sensors effectively measure the magnitude of airflow using different sensing configurations, but they cannot efficiently determine the direction of the airflow since the fiber has cylindrical symmetry.

This letter reports a sensitive directional anemometer that is based on a pendulum-type anisotropic flat-clad tapered fiber Michelson interferometer (AFCTFMI). The structural anisotropy of the AFCTFMI sensor causes the wavelength shifts and visibility of the interference fringes to be correlated with the magnitude and direction of the wind. The proposed in-line directional anemometer can simultaneously and effectively indicate the direction as well as measure the magnitude of the wind.

Figure 1 presents the configuration and operation of the tapered fiber Michelson interferometer (TFMI) for the presented directional anemometer. Here, L represents the length of the pendulum of the fiber cantilever that is fixed by a fiber holder, and is approximately the distance between the

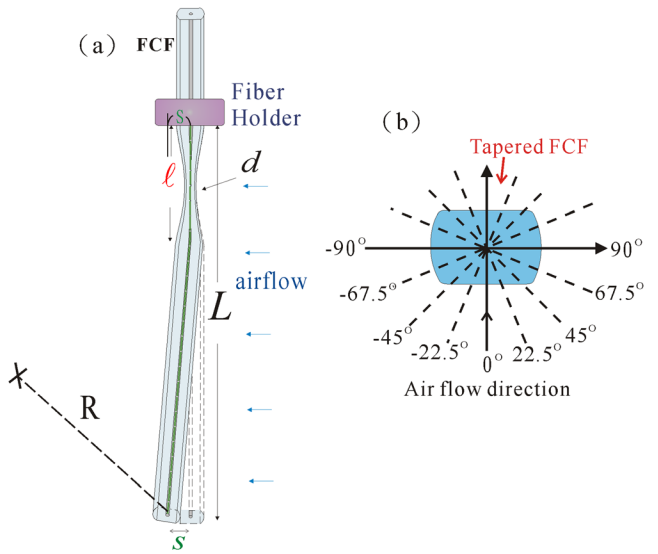

FIG. 1. (a) Configuration and (b) direction of airflow of tapered fiber Michelson interferometer used in proposed directional anemometer.

[a]Email: cherry@nuu.edu.tw.

tapering point and the fiber endface; d is the tapering diameter of fiber, and ℓ is the length of the tapered region. As air flows uniformly to the sensor in different directions, the flowing fluid exerts a force on the fiber pendulum, bending the pendulum and shifting the interference fringes. Figure 1(b) shows the direction of wind. When the airflow acts vertically on the fiber cantilever, a force moment bends the fiber cantilever and deflects the fiber tip with a transverse displacement s. The magnitude of the torque that acts on the fiber tip is proportional to s. The interference mechanism in such TFMI has been demonstrated in Refs. 7, 9, and 10. In the tapered section, light cannot be confined in the core region and the light guidance will be controlled by the cladding-air boundary thus high order cladding modes are excited. When the light propagates into the non-tapered region, the fundamental cladding mode will be transferred to the fundamental core mode but the higher order cladding modes remain in the cladding.[11] These modes are reflected by the fiber endface and interfered in the tapered region. In a small bent angle, cladding mode coupling occurs mainly between LP_{01} and LP_{0m} in the original non-bending taper but particularly between LP_{01} and LP_{1m} in a bending condition.[12] Thus, when the sensor is bent by an acting force, different coupled cladding modes would shift the interference fringes and furthermore evanescent waves stretched much into the air will make a higher loss of the sensor.

In this work, an electrical arc method was utilized to fabricate a taper in a flat-clad fiber (FCF) that is displayed in Fig. 2. The original FCF is only a traditional single-mode fiber with flat-cladding as shown in Fig. 2(a). The fiber taper was fabricated simply using an Ericsson FSU-975 commercial fusion splicer, and as it does not rely on any particular tapering station or precise optical stages. Given an appropriate arc power, arc duration, and stretching distance, the diameter of the fiber was sharpened to a waist diameter of about 36 μm (long axis: d_L) and 24 μm (short axis: d_S) shown in Fig. 2(b) and $\ell \sim 900\,\mu$m (Fig. 2(c)). In Fig. 1, the force that is exerted by the airflow against the fiber arm acts on the pendulum, bending the fiber and deflecting it by a very small deflection s. The value of s is small, so the bending curvature is $C = 1/R \sim 2s/(s^2 + L^2)$. Here, R denotes the radius of bending. The s depends on the force that is exerted by the airflow. Since the shape of the pendulum affects the bending performance of the device, the maximum s can be approximately modeled as stiffness, if L is not too long, as follows:[1]

$$s \sim \frac{4L^4 \rho v^2 C_d}{Ea^3}, \tag{1}$$

where v (m/s) is wind velocity, and $\rho \sim 1.3\,\text{kg/m}^3$ is air density, a represents fiber radius ($2a = d$) and C_d is the drag coefficient which is a function of Reynolds number and is related to the shape of the object on which airflow acts. For airflow velocities between 0.5 and 50 m/s, C_d can be simply assumed to be constant and equal to unity for the fiber.[13] Here, $E \sim 70\,\text{GPa}$ represents Young's modulus of silica, which measures the stiffness of an elastic material under strain or stress.

Based on Eq. (1), the curvature (C) of the bent fiber pendulum can be expressed as

$$C(\theta) \sim \frac{8\rho v^2 C_d L^2 E a^3}{16\rho^2 v^4 C_d^2 L^6 + E^2 a^6} \sim 1.4857 \times 10^{-10} \frac{L^2}{a(\theta)^3} v^2. \tag{2}$$

Equation (2) is a simple form because $E^2 a^6 \gg 16\rho^2 v^4 C_d{}^2 L^6$ at low v, thus $16\rho^2 v^4 C_d{}^2 L^6$ is ignored. Here, the fiber radius $a(\theta)$ and the curvature $C(\theta)$ are directional correlation. In principle, a large C corresponds to a high bending curvature (small bending radius, R) and a highly sensitive sensor. The value of C is almost proportional to v^2 and L^2/a^3, so a fiber cantilever with a larger L and a smaller radius would have greater sensitivity. Based on our experiences, a long fiber pendulum with an L of over 1.5 cm yields an unstable sensing of airflow owing to the ease of vibration and swinging during the measurement, especially in fast flowing air. In this work, the FCF cantilever with $L = 1.4$ cm was used for sensing the direction and magnitude of the wind. Therefore, the corresponding curvatures of the proposed FCF pendulum are determined to be $C_L \sim 0.135v^2$ and $C_S \sim 0.455v^2$ for the

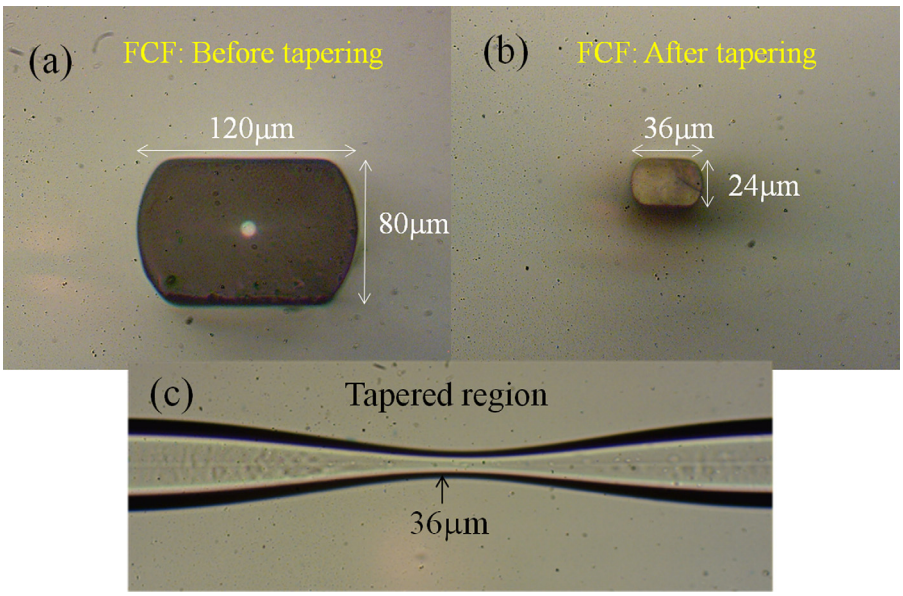

FIG. 2. Cross-sectional micrographs of flat clad fibers (a) before and (b) after tapering with an aspect ratio of about 1.5. (c) Entire tapered region along long axis of the sensor.

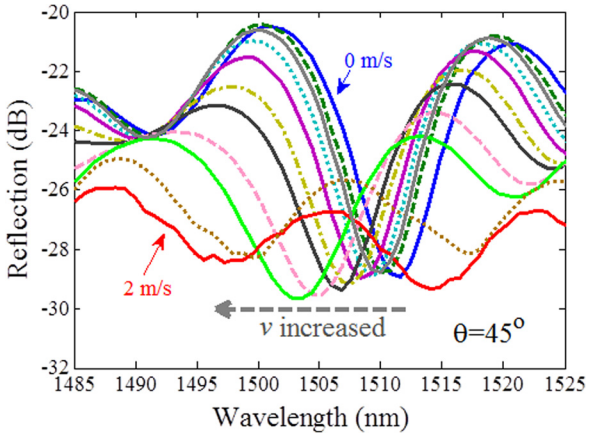

FIG. 3. Interference spectra of proposed sensor with L = 1.4 cm in airflow at various velocities in the direction of $\theta = 45°$.

d_L (long axis; at $\pm 90°$) and d_S (short axis; at 0°) axes on the FCF cross section, respectively.

In the measurement, interference spectra are measured by an optical spectrum analyzer (OSA). Figure 3 presents the interference spectra of the proposed sensor with various wind velocities (0–2 m/s) in a fixed flowing direction of 45°. The interference fringes shift toward shorter wavelengths as the speed of the wind is increased. This figure also reveals poor visibility of the fringes and large spectral losses in a wind with a high velocity. Figure 4(a) plots the wavelength shift versus the velocity of wind in various directions. The highest sensitivity, with a wavelength shift ($\Delta\lambda$) of over 20 nm, is obtained in the wind direction $\theta = 0°$, which corresponds to the thinnest diameter of the tapered fiber cantilever. The inset in Fig. 4(a) shows sensitivity (c_1) related to $\Delta\lambda$, in air that was flowing in different directions, based on the curve fitting relation, $\Delta\lambda = c_1 v^2$. The inset displays the relation between sensitivity (c_1) and wind directions (θ). It can be observed that similar sensitivities were obtained in the symmetrical direction from $-90°$ to 0° because the FCF-based sensor is a bilateral structure. Measured range limited by the structure of the FCF is the main drawback of the device. However, an asymmetrical structure around $0°-360°$ of a fiber can be used as a good candidate for improving this issue.

Figure 4(b) shows that sensitivities of normalized fringe visibility (FV) of the interference patterns to the airflow velocity in various directions. The normalized FV corresponds to a wind velocity of zero on the sensor. A large bending (high v) is associated with poor FV and high loss. Results also indicate that the direction of the wind that blows on the fiber arm strongly affects the FV sensitivity (c_2) of the sensor. The measured range depends on the normalized FV of the range from 1 to zero. In Fig. 4(b), the maximum measurement range is approaching 2 m/s since the interference fringe dip almost vanished (FV closes to zero) which corresponds to the thinnest diameter of the FCF tapered fiber in the condition of $\theta = 0°$.

The inset in Fig. 4(b) plots c_2 for several θ of the wind. Experimental results have demonstrated that the sensitivities of the c_1 and c_2 are quadratically related to wind velocity (v^2), same as shown in Eq. (2). The $\Delta\lambda$ and FV can be obtained from the interference responses for any direction and any speed of wind and the ratio of $\Delta\lambda$ to FV is determined to calculate the normalized sensitivity: $|Nc| \equiv |\Delta\lambda|/|FV|$. The values of $|Nc|$ equal the ratios of $|c_1|$ to $|c_2|$, which are measured and shown in the insets of Figs. 4(a) and 4(b), respectively. Once $|Nc|$ is obtained, the wind direction (θ) can be also determined from the curve in Fig. 4(c) and the magnitude of wind speed can also be then determined from the experimental results of Figs. 4(a) or 4(b). Nevertheless, the sensor certainly is needed to be calibrated and integrated before practical application.

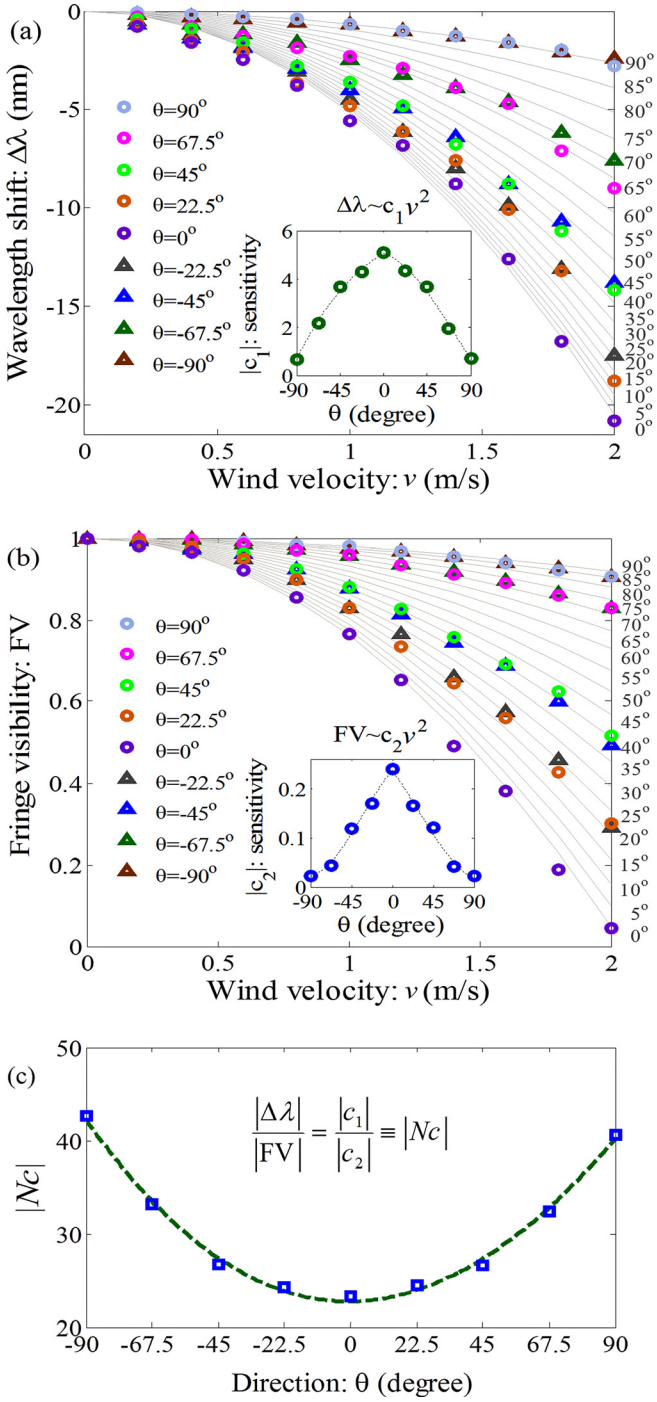

FIG. 4. (a) $\Delta\lambda$ and (b) normalized FV of interference spectra at various velocities with different θ. Insets show sensitivities for various θ. (c) Measurement of normalized sensitivity $|Nc|$ based on the insets in Figs. 4(a) and 4(b) to determine direction of wind.

In conclusion, we have proposed a sensitive directional anemometer based on a pendulum-type of AFCTFMI. The

sensitivity of the AFCTFMI depends on the geometrical structure of the sensing element (diameter and length of fiber cantilever). In particular, it can effectively indicate the direction as well as sensitively measure the magnitude of the wind due to the structural anisotropies of the AFCTFMI. The experimental results show the feasibility of the sensing properties with the optical anisotropy.

This work was partly supported by the National Science Council of the Republic of China under Grant NSC 100-2221-E-239-038.

[1]V. Lien and F. Vollmer, Lab Chip **7**, 1352 (2007).
[2]Y. Zhao, K. Chen, and J. Yang, Measurement **38**, 230 (2005).
[3]S. Takashima, H. Asanuma, and H. Niitsuma, Sens. Actuators, A **116**, 66 (2004).
[4]S. Gao, A. P. Zhang, H. Y. Tam, L. H. Cho, and C. Lu, Opt. Express **19**, 10124 (2011).
[5]D. W. Lamb and A. Hooper, Opt. Lett. **31**, 1035 (2006).
[6]W. N. MacPherson, J. D. C. Jones, B. J. Mangan, J. C. Knight, and P. S. J. Russell, Opt. Commun. **223**, 375 (2003).
[7]L. Yuan, J. Yang, and Z. Liu, IEEE Sens. J. **8**, 1114 (2008).
[8]C. L. Lee, W. Y. Hong, H. J. Hsieh, and Z. Y. Weng, IEEE Photon Technol. Lett. **23**, 905 (2011).
[9]O. Frazão, P. Caldas, F. M. Araújo, L. A. Ferreira, and J. L. Santos, Opt. Lett. **32**, 1974 (2007).
[10]Z. Tian, S. S.-H. Yam, and H.-P. Loock, Opt. Lett. **33**, 1105 (2008).
[11]P.-M. Shankar, L.-C. Bobb, and H.-D. Krumboltz, J. Lightwave Technol. **9**, 832 (1991).
[12]C. Bariain, I. R. Matias. F. J. Arregui, and M. Lopez-Amo, Opt. Eng. **39**, 2241 (2000).
[13]G.-S. Aglietti, J. Aircr. **46**, 2032 (2009).